A structural underpinning of the lower critical solution temperature (LCST) behavior behind temperature-switchable liquids

Ian H. Billinge‡, Gabriel D. Barbosa‡, Songsheng Tao‡, Maxwell Terban, C. Heath Turner*, Simon J. L. Billinge*, Ngai Yin Yip*

Ian H. Billinge – Department of Earth and Environmental Engineering, Columbia University, New York, NY 10027-6623, United States; orcid.org/0000-0002-8475-3952

Gabriel D. Barbosa – Department of Chemical and Biological Engineering, The University of Alabama, Box 870203, Tuscaloosa, AL 35487, USA; orcid.org/0000-0001-7220-9899

Songsheng Tao – Department of Applied Physics and Applied Mathematics, Columbia University, New York, NY 10027-6623, United States; orcid.org/0000-0002-7565-3503

Maxwell Terban –Max Planck Institute for Solid State Research, 70569 Stuttgart, Germany; orcid.org/0000-0002-7094-1266

C. Heath Turner – Department of Chemical and Biological Engineering, The University of Alabama, Box 870203, Tuscaloosa, AL 35487, USA; orcid.org/0000-0002-5707-9480; Email: hturner@eng.ua.edu

Simon J. L. Billinge – Department of Applied Physics and Applied Mathematics, Columbia University, New York, NY 10027-6623, United States; orcid.org/0000-0002-9734-4998; Email: sb2896@columbia.edu

Ngai Yin Yip – Department of Earth and Environmental Engineering, Columbia University, New York, NY 10027-6623, United States; orcid.org/0000-0002-1986-4189; Email: n.y.yip@columbia.edu

ABSTRACT: In this study we use state of the art x-ray scattering and molecular dynamics structural probes to carry out a careful analysis of amine-water mixtures that show the unusual lower critical solution temperature (LCST) behavior. The goal is to provide direct experimental evidence for the entropy-lowering molecular cluster formation originally hypothesized as necessary to LCST behavior. Combined differential wide-angle x-ray scattering and pair distribution analysis, and small angle x-ray scattering measurements were combined with molecular modeling and liquid-liquid equilibrium measurements, revealing direct supporting experimental evidence for the hypothesis. However, the response of the amine phase to accommodating water is even more subtle and interesting than the simple hypothesis suggests, with the formation of robust, nanoscale reverse micelles. The techniques developed in this paper can be expected to yield important insights in the use of temperature-switchable liquids in solvent extraction and other separations. It can also help to explain the stabilization of organelles in living cells that do not have physical membranes but do require compositional gradients to operate.

INTRODUCTION

Biphasic liquid systems are important in many areas of chemistry and biology. For example, in living cells, some organelles do not have membranes and appear to be unbound regions of liquid that sustain different composition and properties to their surroundings.[1] In the chemical industry, biphasic liquids have been used to perform separations for decades.[2,3] Recently, switchable biphasic mixtures have come into focus as an emerging separation method, where the application and removal of a stimulus (*e.g.*, temperature, pH, pressure, light, or CO_2) triggers a drastic change in material properties, such as mutual solubility of two liquids.[4] For example, amine-based switchable solvents have shown potential for desalination,[5–9] water-softening,[10] anti-solvent precipitation,[11] and oil extraction.[12,13]

Amine-water systems are notable for their unusual lower critical solution temperature (LCST; also known as lower consolute solution temperature) behavior: amines are miscible with water at low temperature, combining into a single phase, but separate into two phases at high temperature (for example, see in Figure

2A).[5] Understanding the molecular-level interactions governing the temperature-switchable mixing behavior will enable the informed advancement of these new switchable solvent-based separations, allowing enhanced energy efficiency and improved sustainability.[14]

LCST behavior implies a particular combination of weakly negative enthalpy of mixing, and therefore a thermodynamic tendency to mix at low temperature, combined with negative entropy of mixing, so that a de-mixed, phase separated state becomes favored at higher temperatures. Systems of ideal particles *gain* entropy when mixed: ideal particles have a positive entropy of mixing due to the increase in configurational disorder upon mixing.[15] This would favor mixing over phase-separation at high temperature. Consequently, many biphasic, liquid-liquid systems fully mix only at high temperature, the well-known upper critical solution temperature (UCST) behavior, which is used in chemistry reference texts to explain the role of entropy in phase behavior.[16] Paradoxically, the behavior of LCST systems is the opposite: LCST mixtures become less miscible at high temperatures.

Hirschfelder et al. proposed the first model for LCST systems in 1937,[17] postulating that the unusual behavior was due to strong directional interactions, such as hydrogen bonding, between unlike molecules.[17] In this explanation, at low temperature, molecules of two liquids *A* and *B* form energetically-favorable interactions with one another, producing low-temperature mixing. However, at high temperatures, the system can gain more entropy by phase separating.[17] This is plausible if extended oligomeric structures can form in the mixture that are not present in one or both of the phase separated liquids. Despite the importance of the LCST phenomenon, rigorous studies, with direct experimental evidence for this hypothesis, are lacking.

Modern synchrotron total scattering measurements can give key insights into molecular clustering in liquids.[18] Here we combine modern synchrotron total scattering, small angle x-ray scattering, molecular dynamics, and liquid-liquid equilibrium techniques to look for direct evidence of such dynamic specific molecular clustering in a representative LCST system, mixtures of diisopropylamine (DIPA) and water, across a range of temperatures and mixture compositions.[19] We uncover convincing evidence for the existence of extended, well-defined molecular cluster structures (MCSs) involving DIPA and water. No such well-defined molecular clustering is present in pure DIPA. Thus, the water acts to order the DIPA molecules in the mixture, which will reduce their entropy in the mixture compared to pure, or nearly pure, DIPA. This is direct experimental support for molecular clustering as the source of the negative entropy of mixing that underlies the important LCST phenomenon and yields novel microscopic insights into the origins of the phenomenon.

RESULTS

Our hypothesis is that well-defined, molecular cluster structures (MCSs) of DIPA and water form in DIPA-water mixtures. We test this hypothesis using x-ray total scattering, atomic pair distribution function (PDF) analysis and small-angle x-ray scattering (SAXS), together with molecular modeling and molecular dynamics (MD) simulations.[20,21] Example MCSs are illustrated in Figure 1C. The left-most MCS in Figure 1C shows the basic building block, a DIPA-water dimer, where the oxygen of the water coordinates the nitrogen on the amine through a hydrogen bond. However, we are interested in searching for evidence for larger molecular clusters, as shown in Figure 1C. For example, we show a dumbbell-shaped oligomer of two DIPA molecules with four molecules of water interposed (center). We also show a larger, reverse-micellar structure with multiple DIPAs organized around water in the center (right). In a liquid, should these structures be present, they will not be fully ordered, and indeed will be dynamically forming and breaking. However, if the structures have sufficiently-specific atom-atom coordinations, and persist for sufficient durations, they will yield a signal in the PDF.

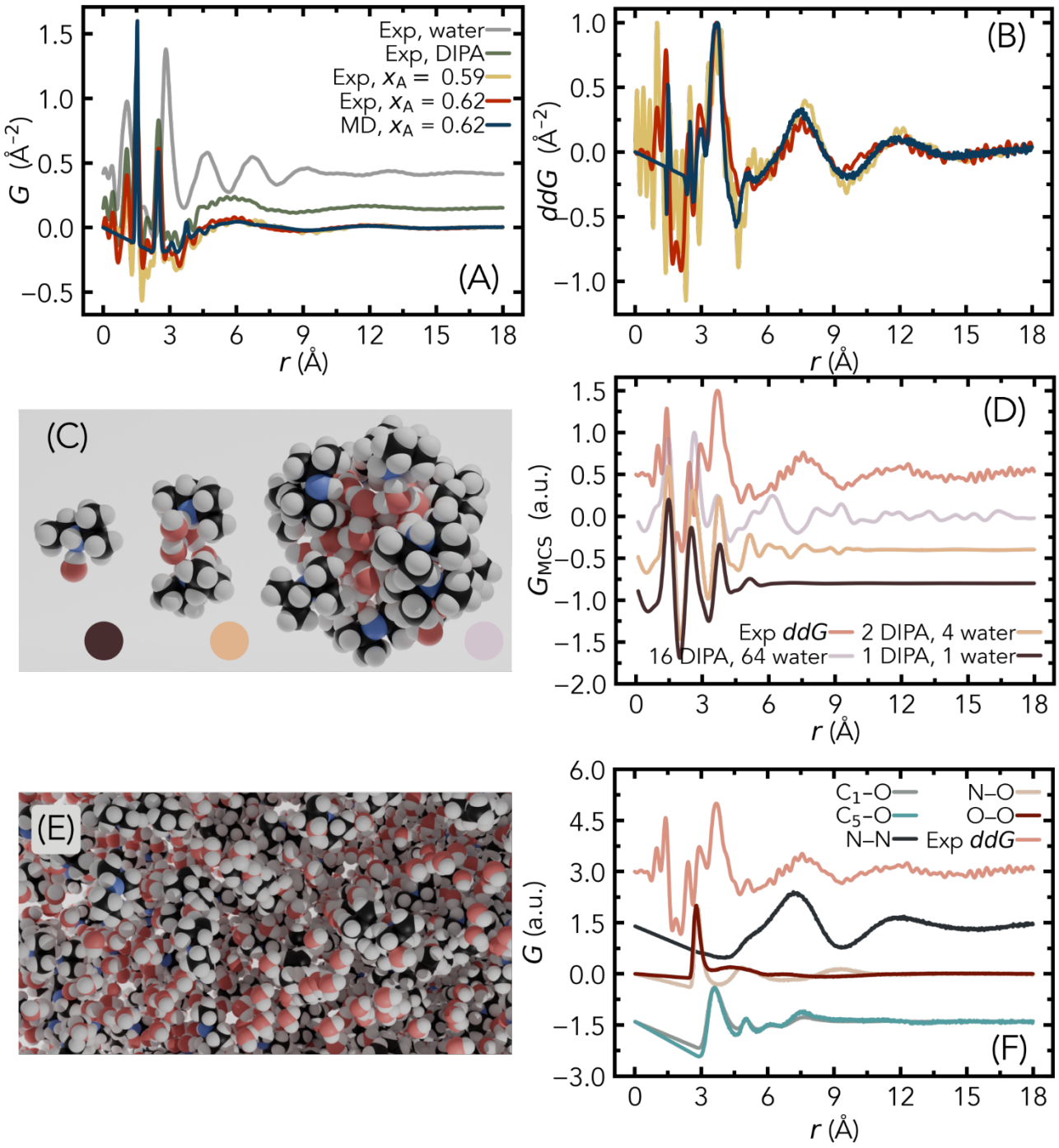

Figure 1. (A) Experimental pair distribution functions, $G(r)$, of water (gray), diisopylamine (green), and a diisopropylamine-water mixture (x_A = 0.62, red, and 0.59, yellow). A pair distribution function generated from MD (x_A = 0.62) is shown in blue. All PDFs are measured or simulated at 25 °C. The experimental PDF of the DIPA-water mixture shows sharp peaks at covalent bond distances (r = 1.5 and 2.5 Å) with little ordering past one molecular distance (~5 Å). (B) Double-differential PDFs of the same experimental and simulated mixtures. Remarkable similarity is apparent between the experimental (red) and MD-derived (blue) ddPDFs. The ddPDFs contain sharp peaks at r = 1.5 and 2.5 Å, arising from imperfect subtraction of intramolecular distances. There follows a peak at r = 2.9 Å, a high, broad peak at centered at r = 3.7 Å, and further broad, triangular peaks at r = 7.5 and 12 Å. (C) Models of small water-DIPA molecular cluster structures (MCSs). Red, black, blue, and white atoms represent oxygen, carbon, nitrogen, and hydrogen, respectively. Left: a single water molecule coordinating a single DIPA molecule.

Middle: Two DIPA molecules with four water molecules forming a dumbbell-like oligomer. Right: a representative reverse micellar structure of 16 DIPA molecules surrounding 64 water molecules. The colored circles indicate the color of the curve in panel D corresponding to each model. (D) PDFs of the molecular cluster structures shown in C. Each PDF shows sharp peaks at low r, representing covalent bonds and second-nearest neighbors in DIPA molecules. The model containing a single DIPA molecule and a single water molecule (brown) also reproduces the features at r = 5.1 and 7.5 Å present in the experimental *ddG*. The experimental *ddG* (red) is plotted for comparison purposes. Larger models (yellow, pink) demonstrate ordering out to higher r, indicating that molecular clustering on a longer length scale is needed to reproduce *ddG*. (E) Representation of an MD ensemble of DIPA and water. (F) MD-derived partial PDFs, $G(r)$, showing interatomic distances for specific pairs of atoms. Carbon-oxygen distances (gray, blue) reproduce features in *ddG* at low r , while nitrogen-nitrogen distances (black) match *ddG* at high r.

The experimentally-accessible PDF is a correlation function that measures the time average of the instantaneous relative positions of atoms in the liquid.[21] An absence of features in this function implies an absence of structural correlations (specific structures), implying a high degree of randomness, and so high entropy. Conversely, the observation of correlations in the PDF signifies the opposite, *i.e.*, order and thus, lower entropy.

The total PDF, *G(r)*, is an average over every interatomic pair in the whole measured sample.[22] We are interested in searching for DIPA-water interactions and higher order MCSs in the DIPA-water mixed phase of the sample, as exemplified in Figure 1C, and mapping these as a function of composition and temperature. To access these signals from the total PDF signal, we have used a double-difference approach, described in detail in the Experimental Section. Briefly, in this approach, we measure the total PDFs of DIPA-water mixtures (Figure 1A, red and yellow) and subtract a linear combination of the pure water and pure DIPA PDFs (Figure 1A, gray and green, respectively). This treatment eliminates the contributions of water molecules coordinating with each other, and likewise DIPA-DIPA correlations. The signal resulting from this approach, the double-differential pair distribution function, which we refer to as *ddG*, is shown in Figure 1B for a representative composition and temperature (red: x_A = 0.62, T = 25 °C, yellow: x_A = 0.59, T = 25 °C).

The *ddG* signal is very small compared to the total PDF (the plots have been rescaled for clarity). However, as demonstrated below, the signals are from the MCSs and are not the result of experimental or data processing errors. We briefly discuss the features in a qualitative way to build understanding. In the total PDFs of the DIPA-water mixture samples (Figure1A, red and yellow), the sharp peaks at 1.5 and 2.5 Å come from covalently-bonded carbon and nitrogen atoms in the DIPA backbone. These appear only vestigially in the *ddG* (as sharp valleys followed by sharp peaks) because they are removed during the subtraction process. Imperfect subtraction of these features is due to a very slight shift in the length of the covalent bonds in the mixture. On the other hand, broad features in the region above 3 Å in the *ddG* (Figure 1B) originate from inter-molecular packing correlations that are present in the mixture but not in the pure liquids. Inter-molecular packing that is disordered and averaged over many different conformations and molecular orientations will result in no signal in the PDF (*i.e.*, a flat line with G = 0 for all r). On the other hand, signals that survive in the *ddG* originate from specific, preferred molecular packings (*i.e.*, molecular cluster structures) that are not dynamically- or ensemble-averaged away. The main features in the *ddG* are strong, broad peaks centered at 3.7, 7.5, and 12 Å. The peaks and valleys are damped with increasing r, monotonically decreasing in amplitude with r. The signal finally disappears at around 20 Å (Figure 1B).

Before interpreting the *ddGs* in more detail, we would like to establish that the signals are, indeed, the PDF of amine-water MCSs in the amine-water mixture and not artifacts of data acquisition and pro-

cessing. We note that the measured *ddG,* (Figure 1B, red and yellow) and that computed from MD simulations (described below, Figure 1B, blue), are very similar. The similarity gives confidence that, on the one hand, the measured signal is originating from the sample and, on the other, that the MD is correctly capturing atomic arrangements in the mixture. We also address a possible concern that the subtraction according to Eq. 2 (Experimental section) did not correctly subtract one of the components. This can be ruled out on the basis that the major features in the *ddG* do not line up with strong peaks in the total PDFs, *G*, of pure water (gray) or pure DIPA (green) in Figure 1A. Thus, features in the *ddG* are only present in the mixture and cannot be attributed to imperfectly subtracted total PDF components. Finally, confidence comes from the fact that the *ddG* is highly reproducible. Measurements taken of different samples with similar compositions, measured months apart at different x-ray beamlines (NSLS-II, 28-ID-1 and 28-ID-2), and in slightly different experimental geometries, yield remarkably similar *ddG* curves (Figure 1B, red and yellow). We can be confident that the signal is intrinsic to the samples.

We next assess whether the *ddG* signal originates from MCSs of the DIPA and water. We study the evolution of the *ddGs* as a function of temperature and composition and show that they evolve as we would expect according to the known DIPA-water phase diagram (**Error! Reference source not found.**A).

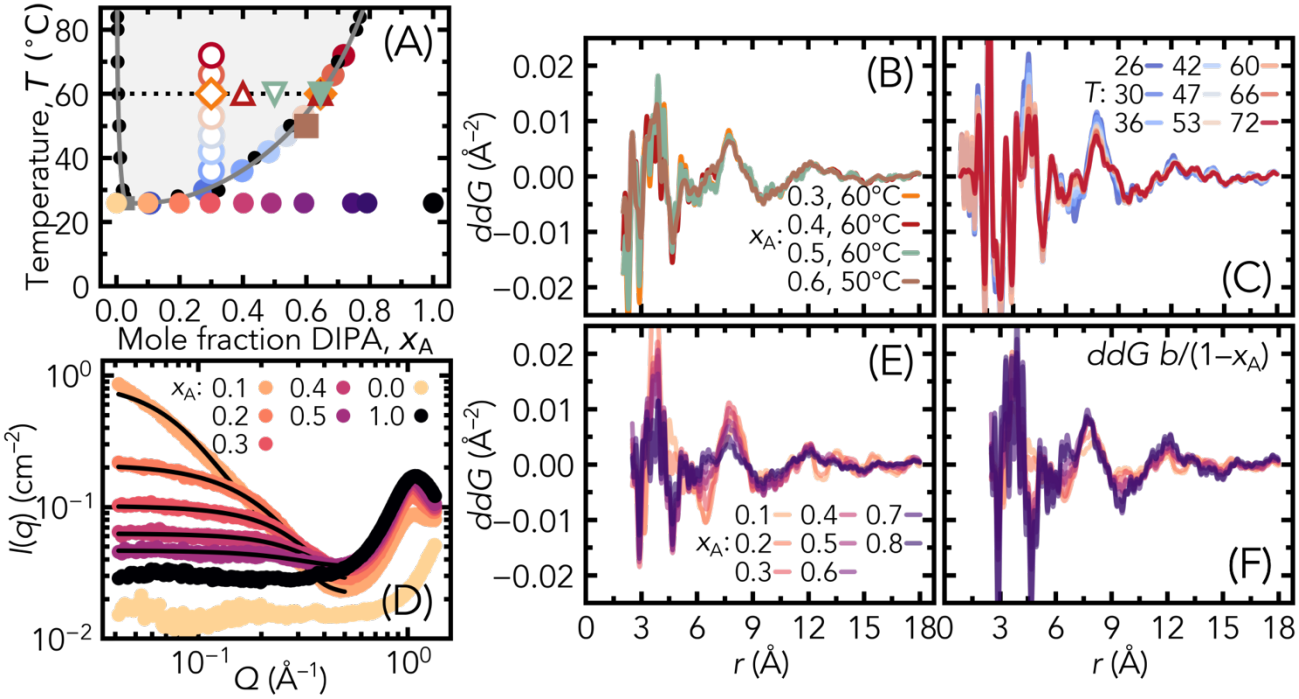

Figure 2. (A) Phase diagram of the DIPA-water system. Phase equilibrium data from Stephenson (black points);[19] fit from Góral et al.[23] The biphasic region (gray area) is delineated by the phase boundary (dark gray curve). The unshaded area indicates the monophasic region. Mixtures with overall compositions in the biphasic liquid region will separate into a water-rich and an amine-rich phase. Overall compositions are shown with hollow points; measured phases are shown with filled points. The 60 °C tie line is indicated by a dotted line. Measured samples are indicated by filled points; if the measured sample is an organic phase of a phase-separated mixture, the composition of the overall mixture is given as a hollow point. (B) *ddG* of the organic phases of three biphasic DIPA-water mixture compositions measured at 60 °C. Orange, red, and green *ddG* curves represent mixtures with overall composition x_A = 0.3, 0.4, and 0.5, whereas the brown curve is the *ddG* of a monophasic mixture (x_A = 0.6, 50 °C). All show remarkable similarity. (C) *ddG* of a biphasic mixture of DIPA and water as a function of temperature (overall com-

position $x_A = 0.3$; organic-phase composition shown with filled points in A). (D) Small-angle x-ray scattering of DIPA-water mixtures measured at 26 °C. Spherical fits are designated by black lines. SAXS fitting results are given in Table S1 of the Supplemental Information. (E) *ddG* of mixtures ranging from $x_A = 0.1$ to 0.8. A significant composition dependence was observable in the broad peaks at 3.7 Å and 7.5 Å and the abutting troughs. (F) The same *ddG* normalized by the mole fraction of water, $x_W = 1 - x_A$, and scaled by an arbitrary factor *b* for visual clarity. This normalization eliminated the composition dependence of the signal, suggesting that the amplitude of the *ddG* signal is a linear function of the mixture composition.

In Figure 2A, the gray shaded region indicates where the mixture separates into water-rich and solvent-rich phases. Outside this region, the mixture is monophasic. In the phase-separated region, at a given temperature (*e.g.*, 60 °C, shown in Figure 2A with a horizontal dotted line), the DIPA-rich phase will always have the same composition regardless of the overall composition of the sample. The composition of the DIPA-rich phase is given by the intersection of the temperature tie-line (dotted line) with the phase boundary (dark gray curve). For example, for $T = 60$ °C, $x_A = 0.644$. The water-rich phase has no signal in the *ddG* and can be neglected, since it either is not intersected by the x-ray beam, or will be subtracted during the difference process. This means that if we measure the PDFs of any nominal composition at 60 °C in the phase-separated region, we would expect to see exactly the same *ddG* signal in each case, that of the DIPA-rich phase with $T = 60$ °C, $x_A = 0.644$. In Figure 2B, we show the *ddG* signals for $x_A = 0.3$, 0.4, and 0.5 (orange, red, and green, respectively) measured at 60 °C. Indeed, the *ddG*s are almost identical to each other, with broad peaks of similar amplitude at 3.7, 7.5, and 12 Å. The *ddG* curves are also very similar to a monophasic sample of similar composition and temperature ($x_A = 0.6$, measured at 50 °C, Figure 2B). The *ddG* signal behaves exactly as we would expect a PDF of a molecular cluster structure, G_{MCS}, to behave in the phase-separated region, giving further confidence that the *ddG* signals are intrinsic to the DIPA-water interactions in the mixture and are representative of features present in water-DIPA molecular clusters.

One important question is whether the molecular structures adopted by DIPA and water vary with the concentration of the mixture in the monophasic region. We plot *ddG* for mixtures of varying concentration ($0.1 \leq x_A \leq 0.8$), all collected at $T = 26$ °C, in Figure 2E. If the structure of the DIPA-water clusters does not change with composition but the number of the clusters increases, we would expect to see the same signal persist but change in amplitude with changing x_A. On the other hand, if the nature of the clusters themselves changes with composition, we would see the shape of the *ddG* signal changing. In the measurements (Figure 2E) we see the same characteristic triangular peaks and valleys in the *ddG* as before, with broad peaks at 3.7 and 7.5 Å, that do not change shape but decrease in amplitude with increasing amine content (or, equivalently, decreasing water content). Apparently, the mixtures adopts the same molecular structures across compositions. Naively, normalizing the curves by the mole fraction of water in the mixture, $x_W = 1 - x_A$ (*i.e.*, plotting $ddG/(1 - x_A)$), might account for the observed changes in amplitude of the *ddG*. The *ddG*s scaled in this way are shown in Figure 2F. Except for $x_A = 0.1$ and 0.2, the curves collapse perfectly on to each other. This is strong evidence that the MCS of DIPA and water are present and do not change significantly in nature with changing concentration for all compositions $x_A \geq 0.3$. The samples with $x_A = 0.1$ and 0.2 gave significantly different signals, but we later ascertained that this was because of phase separation, resulting in the x-ray beam intersecting the aqueous phase instead of the organic phase.

Next, we turn to the evolution of *ddG* with temperature at fixed composition. An example with $x_A = 0.3$ is shown in Figure 2C; similar plots for other compositions are shown Figure S3 in the Supplemental Information. As temperature rises, the mixture will initially remain monophasic. However, once the mixture is heated to its phase separation temperature, 30.9 °C for $x_A = 0.3$, the composition of the organic

phase will evolve, following the phase equilibrium line (Figure 2A, blue and red points). We might expect that, for a given overall mixture composition, *ddG* stays approximately constant with increasing temperature in the monophasic region, but decreases in amplitude on going through the phase separation point as the water content in the DIPA-rich phase decreases. Qualitatively, we see such behavior in the *ddG* signal, as shown in Figures 2C and S3A–D (Supplemental Information). The characteristic *ddG* signal is evident in the data, and we see the amplitude decreasing from lower (bluer hues) to higher (redder hues) temperatures on warming. Indeed, we see a break in the slope of the signal amplitude with T at the phase transition point of 30.9 °C for $x_A = 0.3$. The $x_A = 0.9$ sample never crosses the phase transition line. Correspondingly, there is no change in the signal amplitude as a function of temperature (Figure S3D). For amine contents lower than $x_A = 0.3$, macroscopic phase separation caused the x-ray beam to go through the water-rich and not the DIPA-rich phase, as discussed in the SI, and the *ddG* curves are not meaningful and are not further interpreted.

We now consider the structure of the molecular clusters through modeling. We have taken two approaches to probing structure. One is to use MD simulations of large ensembles of atoms that can sample many different conformations and packing arrangements that might be present in the liquid. The other is to create small molecular clusters directly. These were energy-minimized, as discussed in the Experimental Section, but are not expected to be fully equilibrium structures because the energies are calculated for bare molecular clusters that are not embedded in a background of the liquid. Nonetheless, we can derive interesting insights about the origins of the features in the *ddG* signals in this way, since for both the MD and small-box ensembles, we can calculate the total PDF (the approach for computing the molecular cluster structure PDFs, G_{MCS}s, is described in the Experimental Section).

The smallest molecular cluster we consider is a simple dimer consisting of a water molecule hydrogen-bonded to the nitrogen of DIPA. This is shown as the left-most structure in Figure 1C. The resulting total PDF of this molecular cluster structure, G_{MCS}, is shown as the black curve in Figure 1D. The first two peaks in the G_{MCS} come from the covalent bonds in the DIPA molecule. Strikingly, the model displays peaks at $r = 5.1$ and 7.5 Å (Figure 1D, brown), mirroring the peaks present in *ddG* (reproduced in red in Figure 1D for reference) at the same location. Evidently, *ddG* is capturing water-DIPA dimer interactions at low r. The computed G_{MCS} is for a single arrangement of the atoms. However, the highest-r peak in this dimer model (brown) is at ~5 Å, meaning that G_{MCS} of the dimer cannot explain the intensity that we see in the *ddG* above 5 Å. In other words, larger molecular cluster structures are needed to explain the intensity in the intermediate-r range (5 Å < r < 20 Å).

Accordingly, we considered larger MCSs. One such simple cluster contains two DIPA molecules with four water molecules between them (Figure 1C, middle). In this configuration, a hydrogen bonding network is created through O–N and O–O hydrogen bonds. This G_{MCS} is shown as the beige line in Figure 1D. It displays features in r out to 10 Å, approaching the r-range of the main features at 7.5 and 12 Å, but not to the weak signals seen in the data up to 18 Å. Finally, we consider a more complex MCS with 16 amines and 64 waters (Figure 1C, right). This is the first cluster (grey curve in Figure 1D) we consider which has intensity in G_{MCS} extending to the 8–20 Å, as seen in *ddG*. The arrangement of the MCS is such that a network of hydrogen bonded water molecules at the center is able to hydrogen bond to nitrogen atoms on surrounding DIPA molecules, forming a reverse-micelle like structure.

Summarizing, we can say that minimal MCS models can be built based on simple H-bonding rules, and their G_{MCS}s can be computed. Though the G_{MCS}s are a rough tool for looking at short-range interactions, they are nonetheless easy to make and interpret. The G_{MCS}s here have peaks that are sharper than in the liquid because we have not averaged over different orientations and conformations, but they give insight about the size and possible nature of MCSs that are present in the water-DIPA mixture phase: the *ddG* signal originates from structures based on the dumbbell-like structures where DIPA molecules are separated by interposing water molecules. In this configuration, the DIPA molecules can hydrogen-bonded to

water molecules, and water molecules can form a network of hydrogen bonds among themselves. These can in principle, form reverse micelle like structures if more water molecules interpose between DIPA molecules. We present MD and SAXS evidence below to suggest that formation of inverse micelles is indeed happening in DIPA-water mixtures.

With this insight, we now turn to the MD simulations. Details of the calculations are described in the Experimental Section. After equilibrating the ensembles (a representation is shown in Figure 1E), we calculate total PDFs of the modeled amine-water mixtures. We also equilibrate MD ensembles of pure water and pure DIPA at the same temperatures and pressures, calculate their total PDFs, $G(r)$, and use the modeled pure-component PDFs to extract an MD-derived double differential PDF, $ddG(r)$, according to the same method as the experimental PDFs. As shown by the blue lines in Figure 1A and B, both the MD-derived *G*s and *ddG*s are in excellent agreement with the experimental results. The remarkable agreement of the *ddG*s suggests that the MD simulations reproduced accurate molecular arrangements at the level of the precision of the experimental PDF measurements, giving confidence that we can learn about molecular arrangements from the MD ensembles.

Hydrogen bonding between water and amine is clearly evident in the MD ensembles, as seen from the projection plots of the atomic density around different origin atoms, as shown in Figures S1A–F in the Supplemental Information. The color contour plots show atomic density distributions around a central molecule from the solvent-water mixture with $x_A = 0.42$. Figures S1C and D show a strongly localized atomic density of water around the nitrogen moiety of DIPA, as expected due to hydrogen bond formation. In principle, amines can hydrogen bond to each other with an N–H–N interaction, but the calculations show that this tendency is very weak. There is a slight tendency for DIPA molecules to coordinate one another but the DIPA atomic density around DIPA molecules in the mixture is fairly isotropic, as evident by the generally uniform ring of amine around the central amine molecule (Figures S1A and B). As expected, we do see a strong hydrogen bonding tendency of water around water (Figures S1E and F). The fact that significant water-water hydrogen bonded interactions are present in the MD ensembles of the $x_A = 0.42$ mixture supports the picture that there is significant clustering of water in the mixture despite the two species, water and amine, being present in fairly equal proportion. This is in agreement with our hypothesized DIPA-water-DIPA MCSs.

Figure 1F shows the N–O and O–O partial PDFs computed from MD, G_{NO} and G_{OO}. Both exhibit a first sharp peak at $r = 2.8$ Å, representing N–H–O and O–H–O hydrogen bonding, respectively. These peaks are at almost the same position and have almost the same shape and width as each other. This further signifies that if a water molecule goes into solution in a DIPA-rich phase and replaces an O–H–O hydrogen bond with an O–H–N hydrogen bond, we expect virtually no change in the measured PDF at the position of this peak. This further means that the difference process used to obtain the *ddG* will likely cancel peaks in *ddG* at that location. In other words, the overlap in G_{NO} and G_{NN} at low r explains the lack of a strong hydrogen-bond peak in the *ddG* (Figure 1B).

The N–N partial PDF, G_{NN}, computed between nitrogen atoms in the MD ensemble, is also shown in Figure 1F. G_{NN} has no peak at $r = 2.8$ Å, the position of the hydrogen bond, indicating that there are virtually no direct N–H–N hydrogen bonds in the mixture. Despite this, there are well-defined, broad peaks and valleys in the regions around 7 Å and 12.5 Å that line up quite well with the broad peaks in the *ddG*. This can be explained if the MCSs formed are similar to the DIPA–water–DIPA dumbbells discussed from the small-box modeling above, where nitrogen atoms are held in place relative to each other by well-defined water hydrogen bonding intermediaries.

The presence of clusters of water in the DIPA-water mixture, indicated by the significant O–O coordination at low r in the MD ensembles (Figure 1F), supports the idea that nanoscale regions of water exist

within the amine-water matrix, presumably in the form of reverse micelle-like structures. Several other MD studies have predicted a similar nano-phase separation tendency in amine-water mixtures.[24–26]

To look for direct experimental evidence for these inverse micelle-like structures, we carried out small-angle x-ray scattering (SAXS), a technique that is able to give information on structures between roughly 1 nm and 100 nm in size.[27] Pure liquids are homogeneous down to the nanometer scale and, hence, do not exhibit a SAXS signal. Indeed, the SAXS signals of pure DIPA and pure water (Figure 2D, $x_A = 1.0$ and 0.0, respectively) have no intensity in the low-Q region. The only features of note in the scattering signal of the pure liquids are peaks at around 1 $Å^{-1}$ for pure DIPA and 2 $Å^{-1}$ for pure water, which are the beginning of the wide angle x-ray scattering structure function and encode information about the inter-molecular distances.[28]

However, DIPA-water mixtures with intermediate compositions, measured in the monophasic region (Figure 2D, $x_A = 0.5$, 0.4, 0.3, 0.2, and 0.1, $T = 26$ °C) yield discernable low-Q SAXS features whose prominence grows with increasing water concentration. Water-lean DIPA-water mixtures, on the other hand, show no discernable low-Q scattering (*e.g.*, $x_A = 0.77$, Figure S6) indicating mixture homogeneity. The SAXS measurements were all taken with the system in the monophasic region (compositions and temperatures shown in Figure 2A), so macroscopic phase separation is not a complicating factor. Considering the earlier PDF and MD results, we can hypothesize that this SAXS signal is caused by water segregating into the reverse micelles, and these are embedded within a larger, continuous solvent-rich phase.

In the range $0.2 < x_A < 0.5$, a low-Q plateau emerges. Its intensity increases with increasing water fraction. All these SAXS curves have a "knee" located at around 0.2 $Å^{-1}$, suggesting that the water-DIPA nano-phase-separation is present as nanoscale objects of a quite well-defined size in the DIPA-water mixture. These SAXS curves were best fitted by a model of polydisperse spheres, with a hard sphere structure factor.[27,29,30] This fit returns an average spherical radius parameter, r_{fitted}, and a volume fraction parameter, φ_{fitted}, representing the volume fraction of the mixture occupied by the spheres. The fitting results are detailed in Table S1 of the Supplemental Information, and the best-fit curves are shown as black lines in Figure 1D.

The size of these objects all cluster around a diameter of 16 Å, roughly the size of damping seen in *ddG* and molecular models. Assuming the same density as bulk water, spheres of this fitted size would house around 60-90 water molecules each (calculations presented in Supplemental Information). The SAXS fitting parameters (Figure S4B and C) indicate that there is little change in micelle radius with increasing water content in the mixture (a very slight tendency towards increasing reverse micelle is evident), but there is a strong linear change in φ_{fitted} (Figure S4B; slope = 0.53 ± 0.03, $R^2 = 0.992$). This is in agreement with the x_A-dependence of the *ddG* signal (Figure 2E and F), where the amplitude of *ddG* scales with the water content, indicating that more of the same objects are present with increasing amounts of water. Interestingly, the slope of the fit, 0.53, indicates that the volume occupied by the inverse micelles grows at roughly half the nominal water volume fraction (assuming additive mixing).

For water contents less than 50 mol% (*i.e.*, $x_A > 0.5$), the SAXS signal is very weak. This may suggest that the first MCSs to form just have one or two waters bridging between pairs of DIPAs, much like the simple dumbbell MCS (Figure 1C, middle). Such structures would be visible in the PDF but not in the SAXS since they do not resemble a nanoscale phase separation and therefore a longer-scale heterogeneity in scattering density. The SAXS signal will appear as they form into reverse micelles with a higher water content at the center and a small water content outside. The inverse micelle formation is a mechanism for the DIPA-rich phase to accommodate more water even though the hydrogen bonding requirements of all the DIPA molecules have been satisfied. Rather than excess water molecules being coordinated by DIPA in a non-hydrogen bonded way, the water molecules cluster with each other within the reverse micelles

and gain water-water hydrogen bonding energy while still satisfying all the O–H–N hydrogen bond possibilities.

The MD calculations allow us to interrogate the geometry of the water clusters in the reverse micelles to see if they are modified from pure water. We analyze the three-body angular distributions of water molecules in the MD ensemble. These angular distributions are calculated by averaging the angle formed by each water molecule with two of its four nearest neighbors.[31] The difference between this angular distribution and that of pure water, plotted in Figure S2, demonstrates that there is a small deviation of the structure of water in DIPA-water mixtures compared to that in pure water. Water in the DIPA-water mixtures shows a decreased chance of tetrahedral packing. Surprisingly, as temperature increases, the tetrahedral character of water in the mixture increases: apparently, water molecules in the mixture adopt a structure more like that pure water. This is a larger effect, and an opposite trend, to that reported in previous simulations of the UCST 1-butanol–water mixture.[31]

The SAXS from the sample with $x_A = 0.1$ was not well-fit by the spherical particle model. It shows a very strong small angle scattering signal that does not saturate at low-Q but continues to climb in intensity with decreasing Q (Figure 1D). This is characteristic of small angle scattering from a system without a well-defined size-scale, for example, as would be produced by critical fluctuations approaching a phase transition.[19] Indeed, the $x_A = 0.1$ mixture is very close to the critical point of the mixture, ($x_A = 0.036$, $T = 26$ °C).[23] In this region, thermal fluctuations can be expected to result in large compositional fluctuations on many different length-scales. The fact that this scale-invariant SAXS signal is not seen at other compositions further from the phase line suggests that, although some critical scattering is contributing to the signal in the $x_A = 0.1$ case, the other SAXS signals are not a result of critical scattering since they are qualitatively different in shape. This is strong experimental evidence for the presence of well-defined nano-scale structures in the liquid as we hypothesize.

Discussion

Mixing diisopropylamine and water releases some heat, indicating a small but negative enthalpy of mixing. The negative enthalpy of mixing means that the O–H–N hydrogen bond between water and DIPA has a slightly lower energy than the O–H–O hydrogen bond. This would account for the initial uptake of water into DIPA. However, our results show that, beyond water-DIPA dimers, larger molecular clusters immediately form that resemble dumbbell-like molecular cluster structures. Although in principle N–H–N hydrogen bonds could form between pairs of DIPA molecules in pure DIPA, this does not happen to any great extent, possibly due to steric hindrance.

Because each DIPA has only one nitrogen atom, once such DIPA-water dumbbells form, it is not possible to extend the network further and form larger-scale network structures that would significantly reduce the entropy in the mixed state, the other requirement for LCST behavior. However, the formation of DIPA-water-DIPA clusters will reduce entropy in its own right, much more than simply the formation of DIPA-water dimers, since these larger MCSs will have much higher moment of inertia and be harder to rotate than dimers.

The system can reduce its entropy further, whilst incorporating more water, by interposing more water molecules between DIPAs, forming reverse micelles. In this arrangement, the water molecules also benefit from forming hydrogen bonds with each other, making this a low-energy way of accommodating excess water beyond one-per-DIPA and allowing higher water concentrations in the DIPA-rich phase at little or no energetic cost because the water can form a hydrogen bonded network with itself inside the reverse micelle.

The thermodynamic competition is thus between a monophasic, water-rich mixture of DIPA that includes the micelles, and a biphasic liquid-liquid mixture. In the biphasic liquid mixture, a DIPA-rich phase is in

equilibrium with a macroscopically separate water phase. The phase-separated state has higher entropy because the DIPA phase is much more disordered and has more rotational dynamical degrees of freedom. At high enough temperature, the loss of the O–H–N hydrogen bonds on phase separation is compensated by the increased entropy of phase separation, and the phase-separated state is preferred.

We can speculate on how this might affect the desalination performance of temperature swing solvent extraction, TSSE, one of the applications of switchable amine solvents.[5,8,32] DIPA in contact with a brine at low temperature will take up water from the brine. Our results suggest that initially, this is done through direct hydrogen bonds between the water and the DIPA. Such close coordination between individual water and DIPA molecules is likely to exclude charged salt ions, meaning that water can be extracted from the brine. It is interesting to speculate on what happens when a sufficient amount of water is absorbed into the DIPA-rich phase, allowing inverse micelles to form. On the throughput side, this helps the TSSE process, since more water can be moved out of the brine in each cycle. However, since the water structure at the center of the inverse micelles resembles nano-phase-separated water, we might speculate that salt could also be accommodated into the micelles, a phenomenon that could give rise to the salt selectivity-water productivity tradeoff seen in TSSE.[33] A better understanding of the structure of amine-water-salt mixtures can help us to develop and select solvents that optimize the balance between throughput and selectivity.[34] Similar arguments apply to the case where solvents are being used for ion extraction from water.

We believe that the insights from this work may also have implications in biology. In cells, proteins and their constituent amino acids are ubiquitous in aqueous solutions.[35] Structuring is all-important to protein function and is strongly dependent on the surrounding solvent environment.[36] New insights into the interplay between proteins and their surroundings is key to biological understanding. In fact, some cellular organelles are unbound by membranes and apparently exist as stable liquid regions of substantially different composition than their surroundings.[1] The amine-water mixture studied here can be a model system for studying compositional fluctuations caused by water-amino chemistry.

Since the local structure of complex mixtures can show effects that are not explained by continuum models of solvents, studies such as the current one can be expected to lead to a greater understanding of solvent mixture systems.[37] The orientation of molecules around one another, hydrogen bonding structure, and longer-range aggregation all have strong impacts on the local environment experienced by a species in a mixture.[37] For example, conditions at the sub-nanometer scale may alter the immediate region around interfaces, catalytic sites, and minority species in solution, and have a strong bearing on the behavior of a mixture.[38] Our novel application of double-differential pair distribution function analysis to biphasic liquids over wide ranges of composition and temperature has shown to give reproducible results, despite the weak signals, and is a powerful method for studying molecular interactions inside such complex systems. In particular, we found that, even at low water loading, DIPA-water mixtures showed signs of structuring. Whilst very careful and detailed models of solvation have been developed using diffraction methods and large-scale models on model systems, for example through the determination of partial PDFs with the use of selective deuteration,[39,40] our approach of rapid measurements of entire phase diagrams, combining multiple complementary measurements, combined with modeling ideal clusters and bulk systems, can give critical insights that are difficult to extract in other ways.

Extending this idea, and highly relevant for understanding switchable solvents and their performance, making measurements that give insight into the structure and dynamics of local chemical environments as they respond to stimuli helps inform the selection and application of the reversible solvents.[34] The techniques developed here would be well-suited to further study of other switchable solvents, ionic liquids, deep eutectic solvents, polymers, microemulsions, supramolecular chemistries, and nanomaterials.

Experimental Section

Pair Distribution Function

Pair distribution function experiments were carried out at Beamline 28-ID-1 and 28-ID-2 at National Synchrotron Light Source II (Brookhaven National Laboratory, NY, USA), using the rapid acquisition PDF method (RAPDF).[41] A 2-dimensional amorphous silicon detector (PerkinElmer, Waltham, MA, USA) was placed 211 mm behind the samples, which were loaded in nuclear magnetic resonance tubes of 3 mm outer diameter (Bruker Corporation, Billerica, MA, USA). The incident wavelength of the x-rays utilized was 0.1847 Å. Calibration of the experimental setup was done using nickel powder.

Datasets were collected at nine temperatures between 25 and 72 °C. Raw data was summed and corrected for polarization effects before being integrated along arcs of constant angle to produce 1-dimensional powder diffraction patterns using the program pyFAI.[42] The resulting intensity distributions had non-structural contributions to the data removed and were divided by the average atomic form factor squared before being normalized to obtain, $F(q)$. This process was done using the *ad hoc* algorithms in PDFgetX3, which was also used to carry out the Fourier transform to obtain the PDF, $G(r)$.[43] The maximum amplitude of the scattering vector, Q, used in the Fourier transform was 22.0 $Å^{-1}$.

PDFs of multicomponent mixtures (e.g., water and amine solvent) include information from interactions between atoms within molecules, between molecules of the same species, and between molecules of different species. The double-differential PDF (*ddG*) technique extracts information about interactions that arise only in mixtures.[44–46] For amine-water mixtures, the PDF, G_{mix}, consists of three contributions,

$$G_{mix}(r) = G_A(r) + G_W(r) + G_{AW}(r), \quad (1)$$

where G_A and G_W represent amine-amine and water-water interactions respectively. G_{AW} represents interatomic distances between amine and water molecules and reveals the spatial correlation between the two species in the mixture. The pure component PDFs may then be subtracted from the mixture PDF to obtain the double differential PDF, $ddG(r)$,

$$ddG(r) = G_{mix}(r) - a_A G_A(r) - a_W G_W(r). \quad (2)$$

The coefficients a_A and a_W are determined as

$$a_A, a_W = \text{argmin}_{a_A', a_W'} |G_{mix}(r) - a_A' G_A(r) - a_W' G_W(r)|^2. \quad (3)$$

In simple terms, a_A and a_W are fitting parameters that minimize the residual signal (Eq 3). The double differential PDF signal, $ddG(r)$, is representative of interatomic distances that either arise only in the mixture (e.g., amine-water interactions) or change substantially in the mixture (e.g., altered water-water or amine-amine interactions). The interaction of interest between amine and water molecules, G_{AW}, is expected to be eclipsed by the substantially stronger amine-amine and water-water signals in the total PDF, whereas the double differential PDF analysis adroitly uncovers the subtle but important G_{AW} signals to shed light on the molecular-level interactions that arise only in the mixture.

Molecular Dynamics

Gromacs 2021.1 was used to perform MD simulations.[47,48] Packmol was used to build initial configurations.[49] Bonded and non-bonded interactions of the amine solvents were modeled using the OPLS-AA force field.[50,51] Water was modeled using the TIP4P model.[52] LigParGen with the 1.14*CM1A-LBCC charge method was used to obtain atomic partial charges and OPLS-AA parameters.[53,54] Following the approach of the force field used herein, geometric combination rules were used to model unlike-pair interactions. A cut-off radius of 10 Å was used for van der Waals interactions, and the Particle Mesh Ewald

Simulation parameters of composition, temperature, and pressure were chosen to match experimental conditions. Based on the initial configuration, the steepest descent method was used to minimize the energy of the system, followed by an initial equilibration of 15 ns, in which temperature and pressure were kept constant by using the v-rescale thermostat and Parrinello-Rahman barostat algorithm, respectively.[55–57] Following equilibration, an additional 5.0 ns were used for sampling. Periodic boundary conditions were applied in the *x*, *y*, and *z* directions, and the leapfrog algorithm was used to integrate the equation of motion with a time step of 2 fs. Hydrogen bonds were constrained using the LINCS algorithm.[58] Radial distribution functions (RDFs) and hydrogen bond analyses were obtained using Gromacs built-in analysis tools. Finally, Travis was used to obtain the water-water and solvent-water plane projection distribution (PPD).[59,60] The *ddG* technique described above was also applied to the PDFs generated by MD simulations, allowing comparisons between computationally- and experimentally-derived *ddG*s.

Small Molecular Cluster Models

Model systems were created in Avogadro 1.2.0.[61] The models were equilibrated using the built-in energy minimization feature in Avogadro, using the MMFF94s force field.[62] PDFs were generated from the models using the DebyePDFCalculator class from diffpy-cmi.[63] Isotropic atomic displacement parameters, $B_{iso} = 8\pi^2 U_{iso}$, were set to 2 Å^2 for each atom type. Q_{min}, Q_{max}, Q_{damp}, and Q_{broad} were set to 0, 25, 0, and 0 Å^{-1}, respectively.

Small-Angle X-Ray Scattering

Small-angle x-ray scattering (SAXS) can characterize nano-scale structures in liquids.[27,64] SAXS was employed in this study to assess size and shape of such structures in amine-water mixtures. SAXS experiments were performed using a Xenocs Genix 3D instrument (Sassenage, France) in medium-angle (0.02–0.07 Å^{-1}), and wide-angle scattering (0.07–2.7 Å^{-1}) configurations. Samples of amine-water mixtures were contained inside 1.0 mm inner diameter glass capillary tubes procured from Charles Supper, Co. (Westborough, MA, USA) and sealed with amine-compatible epoxy. A low-*Q* cutoff was applied to scattering data based on inspection of scattering patterns, to eliminate regions where the experimental artefact of beamstop scattering was apparent. Background correction was then performed by subtracting the scattering from an empty capillary tube. The wavelength, λ, of the incident x-ray beam was 1.54 Å. Experiments at ambient temperature were performed at 26 °C inside the instrument (i.e., without active temperature control). SAXS fitting was performed using SasView 5.0.4.[65] A spherical model with a hard-sphere structure factor was used for all samples (details available in the Supplemental Information).[27,29,30]

AUTHOR INFORMATION

Corresponding Author

* Ngai Yin Yip – Fu Foundation Columbia School of Engineering and Applied Science, New York, NY 10027, United States; orcid.org/0000-0002-1986-4189; Email: n.y.yip@columbia.edu

*Simon J. L. Billinge – Fu Foundation Columbia School of Engineering and Applied Science, New York, NY 10027, United States; orcid.org/0000-0002-9734-4998; Email: sb2896@columbia.edu

* C. Heath Turner –The University of Alabama, Tuscaloosa, AL 35487, USA; orcid.org/0000-0002-5707-9480; Email: hturner@eng.ua.edu

ACKNOWLEDGMENTS

The authors thank Sanjit Ghose for help with synchrotron experiments including designing and constructing a temperature stage. I.H.B thanks Kinnari, M. Shah, Eliza Dach, and Sherry Zhang for useful conversations. I.H.B. thanks Marshall Tekell for help with small-angle x-ray scattering measurements. Work in Yip Lab was based upon work supported by the U.S. Department of Energy, Office of Science, Basic Energy Sciences under Award Number DE-SC0024574. Work in the Billinge-group in the Applied Physics and Applied Mathematics Department was supported by U.S. Department of Energy, Office of Science, Office of Basic Energy Sciences (DOE-BES) under contract No. DE-SC0024141. C.H.T. acknowledges support from the U.S. Bureau of Reclamation, No. R23AC00435.

Declaration of Interests

Ngai Yin Yip is a co-founder and chief technical officer of Trident Desalination. Ian Billinge and Ngai Yin Yip are holders of patents relating to temperature swing solvent extraction. The other authors declare no competing interests.

REFERENCES

(1) Hyman, A. A.; Weber, C. A.; Jülicher, F. Liquid-Liquid Phase Separation in Biology. *Annu. Rev. Cell Dev. Biol.* **2014**, *30* (1), 39–58. https://doi.org/10.1146/annurev-cellbio-100913-013325.

(2) Seader, J. D.; Henley, E. J.; Roper, D. K. *Process Separation Principles with Applications Using Process Simulators*, 4th ed.; Wiley, 2016.

(3) Kiss, A. A.; Lange, J.-P.; Schuur, B.; Brilman, D. W. F.; van der Ham, A. G. J.; Kersten, S. R. A. Separation Technology–Making a Difference in Biorefineries. *Biomass Bioenergy* **2016**, *95*, 296–309. https://doi.org/10.1016/j.biombioe.2016.05.021.

(4) Jessop, P. G.; Heldebrant, D. J.; Li, X.; Eckert, C. A.; Liotta, C. L. Reversible Nonpolar-to-Polar Solvent. *Nature* **2005**, *436* (7054), 1102–1102. https://doi.org/10.1038/4361102a.

(5) Foo, Z. H.; Stetson, C.; Dach, E.; Deshmukh, A.; Lee, H.; Menon, A. K.; Prasher, R.; Yip, N. Y.; Lienhard, J. H.; Wilson, A. D. Solvent-Driven Aqueous Separations for Hypersaline Brine Concentration and Resource Recovery. *Trends Chem.* **2022**, *4* (12), 1078–1093. https://doi.org/10.1016/j.trechm.2022.09.004.

(6) Davidson, R. R.; Smith, W. H.; Hood, D. W. Structure and Amine-Water Solubility in Desalination by Solvent Extraction. *J. Chem. Eng. Data* **1960**, *5* (4), 420–423. https://doi.org/10.1021/je60008a005.

(7) Davison, R. R.; Harris, W. B.; Smith, W. H. A Solvent Extraction Desalination Pilot Plant. *Desalination* **1967**, *3* (1), 17–26. https://doi.org/10.1016/S0011-9164(00)84020-5.

(8) Boo, C.; Winton, R. K.; Conway, K. M.; Yip, N. Y. Membrane-Less and Non-Evaporative Desalination of Hypersaline Brines by Temperature Swing Solvent Extraction. *Environ. Sci. Technol. Lett.* **2019**, *6* (6), 359–364. https://doi.org/10.1021/acs.estlett.9b00182.

(9) Boo, C.; Billinge, I. H.; Chen, X.; Shah, K. M.; Yip, N. Y. Zero Liquid Discharge of Ultrahigh-Salinity Brines with Temperature Swing Solvent Extraction. *Environ. Sci. Technol.* **2020**, *54* (14), 9124–9131. https://doi.org/10.1021/acs.est.0c02555.

(10) Boo, C.; Qi, H.; Billinge, I. H.; Shah, K. M.; Fan, H.; Yip, N. Y. Thermomorphic Hydrophilicity Base-Induced Precipitation for Effective Descaling of Hypersaline Brines. *ACS EST Eng.* **2021**, *1* (9), 1351–1359. https://doi.org/10.1021/acsestengg.1c00160.

(11) Wallace, W. T.; Hayward, J. S.; Ho, C.-Y.; Marsh, A. R.; Tariq, A.; Bartley, J. K. Triethylamine–Water as a Switchable Solvent for the Synthesis of Cu/ZnO Catalysts for Carbon Dioxide Hydrogenation to Methanol. *Top. Catal.* **2021**, *64* (17), 984–991. https://doi.org/10.1007/s11244-021-01457-6.

(12) Li, X.; Hou, J.; Sui, H.; Sun, L.; Xu, L. Switchable-Hydrophilicity Triethylamine: Formation and Synergistic Effects of Asphaltenes in Stabilizing Emulsions Droplets. *Materials* **2018**, *11* (12), 2431. https://doi.org/10.3390/ma11122431.

(13) Vanderveen, J. R.; Geng, J.; Zhang, S.; Jessop, P. G. Diamines as Switchable-Hydrophilicity Solvents with Improved Phase Behaviour. *RSC Adv.* **2018**, *8* (48), 27318–27325. https://doi.org/10.1039/C8RA05751F.

(14) *The Application of Green Solvents in Separation Processes*; Pena-Pereira, F., Tobiszewski, M., Eds.; Elsevier, 2017.

(15) Atkins, P. W. *Physical Chemistry*, 4th ed.; W.H. Freeman and Company: New York, 1990.

(16) Chemistry (IUPAC), T. I. U. of P. and A. *IUPAC - upper critical solution temperature (UT07280)*. https://doi.org/10.1351/goldbook.UT07280.

(17) Hirschfelder, J.; Stevenson, D.; Eyring, H. A Theory of Liquid Structure. *J. Chem. Phys.* **1937**, *5* (11), 896–912. https://doi.org/10.1063/1.1749960.

(18) Head-Gordon, T.; Hura, G. Water Structure from Scattering Experiments and Simulation. *Chem. Rev.* **2002**, *102* (8), 2651–2670. https://doi.org/10.1021/cr0006831.

(19) Stephenson, R. M. Mutual Solubility of Water and Aliphatic Amines. *J. Chem. Eng.*

Data **1993**, *38* (4), 625–629. https://doi.org/10.1021/je00012a039.
(20) Terban, M. W.; Billinge, S. J. L. Structural Analysis of Molecular Materials Using the Pair Distribution Function. *In Prep.* **2021**.
(21) Billinge, S. J. L.; Jensen, K. M. Ø. *Atomic Pair Distribution Function Analysis: A Primer*, 1st ed.; IUCr Texts on Crystallography; Oxford Science Publishers, 2024.
(22) Egami, T.; Billinge, S. J. L. *Underneath the Bragg Peaks: Structural Analysis of Complex Materials*; Pergamon Press, Elsevier: Oxford, England, 2003.
(23) Góral, M.; Shaw, D. G.; Mączyński, A.; Wiśniewska-Gocłowska, B.; Oracz, P. IUPAC-NIST Solubility Data Series. 96. Amines with Water Part 1. C4–C6 Aliphatic Amines. *J. Phys. Chem. Ref. Data* **2012**, *41* (4), 043106. https://doi.org/10.1063/1.4755288.
(24) Sappidi, P.; Barbosa, G.; Rabideau, B. D.; Weinman, S. T.; Turner, C. H. Molecular Simulation of High-Salinity Brines in Contact with Diisopropylamine and Tripropylamine Solvents. *Ind. Eng. Chem. Res.* **2021**, *60* (21), 7917–7925. https://doi.org/10.1021/acs.iecr.1c01057.
(25) Barbosa, G. D.; Liu, X.; Bara, J. E.; Weinman, S. T.; Turner, C. H. High-Salinity Brine Desalination with Amine-Based Temperature Swing Solvent Extraction: A Molecular Dynamics Study. *J. Mol. Liq.* **2021**, *341*, 117359. https://doi.org/10.1016/j.molliq.2021.117359.
(26) Barbosa, G. D.; Dach, E.; Liu, X.; Yip, N. Y.; Turner, C. H. Computational and Experimental Study of Different Brines in Temperature Swing Solvent Extraction Desalination with Amine Solvents. *Desalination* **2022**, *537*, 115863. https://doi.org/10.1016/j.desal.2022.115863.
(27) Guinier, A.; Fournet, G. *Small-Angle Scattering of X-Rays*; Wiley: New York, 1955.
(28) Hura, G.; Russo, D.; M. Glaeser, R.; Head-Gordon, T.; Krack, M.; Parrinello, M. Water Structure as a Function of Temperature from X-Ray Scattering Experiments and Ab Initio Molecular Dynamics. *Phys. Chem. Chem. Phys.* **2003**, *5* (10), 1981–1991. https://doi.org/10.1039/B301481A.
(29) Kotlarchyk, M.; Chen, S. Analysis of Small Angle Neutron Scattering Spectra from Polydisperse Interacting Colloids. *J. Chem. Phys.* **1983**, *79* (5), 2461–2469. https://doi.org/10.1063/1.446055.
(30) Percus, J. K.; Yevick, G. J. Analysis of Classical Statistical Mechanics by Means of Collective Coordinates. *Phys. Rev.* **1958**, *110* (1), 1–13. https://doi.org/10.1103/PhysRev.110.1.
(31) Robinson Brown, D. C.; Webber, T. R.; Jiao, S.; Rivera Mirabal, D. M.; Han, S.; Shell, M. S. Relationships between Molecular Structural Order Parameters and Equilibrium Water Dynamics in Aqueous Mixtures. *J. Phys. Chem. B* **2023**, *127* (20), 4577–4594. https://doi.org/10.1021/acs.jpcb.3c00826.
(32) Davison, R. R.; Smith, W. H.; Hood, D. W. Structure and Amine-Water Solubility in Desalination by Solvent Extraction. *J. Chem. Eng. Data* **1960**, *5* (4), 420–423. https://doi.org/10.1021/je60008a005.
(33) Shah, K. M.; Dach, E.; Winton, R.; Fan, H.; Yip, N. Y. Phase Equilibria Insights into Amine-Water-NaCl Interactions in Liquid-Liquid Biphasic Systems for Temperature Swing Solvent Extraction Desalination. *Desalination* **2023**, *548*, 116259. https://doi.org/10.1016/j.desal.2022.116259.
(34) Barbosa, G. D.; Turner, C. H. Computational Assessment of an Amine-Based Solvent Library for High-Salinity Brine Desalination. *Ind. Eng. Chem. Res.* **2023**, *62* (20), 8033–8041. https://doi.org/10.1021/acs.iecr.3c00879.
(35) McLain, S. E.; Soper, A. K.; Terry, A. E.; Watts, A. Structure and Hydration of L-Proline in Aqueous Solutions. *J. Phys. Chem. B* **2007**, *111* (17), 4568–4580. https://doi.org/10.1021/jp068340f.
(36) Zhang, Y.; Cremer, P. S. Interactions between Macromolecules and Ions: The Hofmeister Series. *Curr. Opin. Chem. Biol.* **2006**, *10* (6), 658–663. https://doi.org/10.1016/j.cbpa.2006.09.020.
(37) Collins, K. D. Why Continuum Electrostatics Theories Cannot Explain Biological Structure, Polyelectrolytes or Ionic Strength Effects in Ion–Protein Interactions. *Biophys.*

Chem. **2012**, *167*, 43–59. https://doi.org/10.1016/j.bpc.2012.04.002.
(38) Argyris, D.; Tummala, N. R.; Striolo, A.; Cole, D. R. Molecular Structure and Dynamics in Thin Water Films at the Silica and Graphite Surfaces. *J. Phys. Chem. C* **2008**, 13587–13599.
(39) Soper, A. K.; Phillips, M. G. A New Determination of the Structure of Water at 25°C. *Chem. Phys.* **1986**, *107* (1), 47–60. https://doi.org/10.1016/0301-0104(86)85058-3.
(40) Soper, A. K.; Weckström, K. Ion Solvation and Water Structure in Potassium Halide Aqueous Solutions. *Biophys. Chem.* **2006**, *124* (3), 180–191. https://doi.org/10.1016/j.bpc.2006.04.009.
(41) Chupas, P. J.; Qiu, X.; Hanson, J. C.; Lee, P. L.; Grey, C. P.; Billinge, S. J. L. Rapid-Acquisition Pair Distribution Function (RA-PDF) Analysis. *J. Appl. Crystallogr.* **2003**, *36* (6), 1342–1347. https://doi.org/10.1107/S0021889803017564.
(42) Kieffer, J.; Wright, J. P. PyFAI: A Python Library for High Performance Azimuthal Integration on GPU. *Powder Diffr.* **2013**, *28* (S2), S339–S350. https://doi.org/10.1017/S0885715613000924.
(43) Juhas, P.; Davis, T.; Farrow, C. L.; Billinge, S. J. L. PDFgetX3: A Rapid and Highly Automatable Program for Processing Powder Diffraction Data into Total Scattering Pair Distribution Functions. *J. Appl. Crystallogr.* **2013**, *46* (2), 560–566. https://doi.org/10.1107/S0021889813005190.
(44) Li, W.; Harrington, R.; Tang, Y.; Kubicki, J. D.; Aryanpour, M.; Reeder, R. J.; Parise, J. B.; Phillips, B. L. Differential Pair Distribution Function Study of the Structure of Arsenate Adsorbed on Nanocrystalline γ-Alumina. *Environ. Sci. Technol.* **2011**, *45* (22), 9687–9692. https://doi.org/10.1021/es200750b.
(45) Chapman, K. W.; Chupas, P. J.; Kepert, C. J. Selective Recovery of Dynamic Guest Structure in a Nanoporous Prussian Blue through in Situ X-Ray Diffraction: A Differential Pair Distribution Function Analysis. *J. Am. Chem. Soc.* **2005**, *127* (32), 11232–11233. https://doi.org/10.1021/ja053266k.
(46) Sprouster, D. J.; Snead, L. L.; Dooryhee, E.; Ghose, S. K.; Koyanagi, T.; Katoh, Y. Pair Distribution Function Analysis of Neutron-Irradiated Silicon Carbide. *J. Nucl. Mater.* **2019**, *527*, 151798. https://doi.org/10.1016/j.jnucmat.2019.151798.
(47) Lindahl; Abraham; Hess; Spoel, van der. GROMACS 2021.1 Manual. **2021**. https://doi.org/10.5281/ZENODO.4561625.
(48) Lindahl; Abraham; Hess; Spoel, van der. GROMACS 2021.1 Source Code. **2021**. https://doi.org/10.5281/ZENODO.4561626.
(49) Martinez, L.; Andrade, R.; Birgin, E. G.; Martinez, J. M. PACKMOL: A Package for Building Initial Configurations for Molecular Dynamics Simulations. *J. Comput. Chem.* **2009**, *30* (13), 2157–2164.
(50) Jorgensen, W. L.; Maxwell, D. S.; Tirado-Rives, J. Development and Testing of the OPLS All-Atom Force Field on Conformational Energetics and Properties of Organic Liquids. *J. Am. Chem. Soc.* **1996**, *118* (45), 11225–11236.
(51) Jorgensen, W. L.; Tirado-Rives, J. The OPLS Force Field for Proteins. Energy Minimizations for Crystals of Cyclic Peptides and Crambin. *J. Am. Chem. Soc.* **1988**, *110* (6), 1657–1666.
(52) Jorgensen, W. L.; Chandrasekhar, J.; Madura, J. D.; Impey, R. W.; Klein, M. L. Comparison of Simple Potential Functions for Simulating Liquid Water. *J. Chem. Phys.* **1983**, *79* (2), 926–935. https://doi.org/10.1063/1.445869.
(53) Dodda, L. S.; de Vaca, I.; Tirado-Rives, J.; Jorgensen, W. L. LigParGen Web Server: An Automatic OPLS-AA Parameter Generator for Organic Ligands. *Nucleic Acids Res.* **2017**, *45* (W1), W331--W336.
(54) Dodda, L. S.; Vilseck, J. Z.; Tirado-Rives, J.; Jorgensen, W. L. 1.14* CM1A-LBCC: Localized Bond-Charge Corrected CM1A Charges for Condensed-Phase Simulations. *J. Phys. Chem. B* **2017**, *121* (15), 3864–3870.

(55) Bussi, G.; Donadio, D.; Parrinello, M. Canonical Sampling through Velocity Rescaling. *J. Chem. Phys.* **2007**, *126* (1), 14101.
(56) Nosé, S.; Klein, M. L. Constant Pressure Molecular Dynamics for Molecular Systems. *Mol. Phys.* **1983**, *50* (5), 1055–1076.
(57) Parrinello, M.; Rahman, A. Polymorphic Transitions in Single Crystals: A New Molecular Dynamics Method. *J. Appl. Phys.* **1981**, *52* (12), 7182–7190.
(58) Hockney, R. W.; Goel, S. P.; Eastwood, J. W. Quiet High-Resolution Computer Models of a Plasma. *J. Comput. Phys.* **1974**, *14* (2), 148–158. https://doi.org/10.1016/0021-9991(74)90010-2.
(59) Brehm, M.; Thomas, M.; Gehrke, S.; Kirchner, B. TRAVIS—A Free Analyzer for Trajectories from Molecular Simulation. *J. Chem. Phys.* **2020**, *152* (16), 164105. https://doi.org/10.1063/5.0005078.
(60) Brehm, M.; Kirchner, B. TRAVIS - A Free Analyzer and Visualizer for Monte Carlo and Molecular Dynamics Trajectories. *J. Chem. Inf. Model.* **2011**, *51* (8), 2007–2023. https://doi.org/10.1021/ci200217w.
(61) Hanwell, M. D.; Curtis, D. E.; Lonie, D. C.; Vandermeersch, T.; Zurek, E.; Hutchison, G. R. Avogadro: An Advanced Semantic Chemical Editor, Visualization, and Analysis Platform. *J. Cheminformatics* **2012**, *4* (1), 17. https://doi.org/10.1186/1758-2946-4-17.
(62) Halgren, T. A. MMFF VI. MMFF94s Option for Energy Minimization Studies. *J. Comput. Chem.* **1999**, *20* (7), 720–729. https://doi.org/10.1002/(SICI)1096-987X(199905)20:7<720::AID-JCC7>3.0.CO;2-X.
(63) Juhás, P.; Farrow, C. L.; Yang, X.; Knox, K. R.; Billinge, S. J. L. Complex Modeling: A Strategy and Software Program for Combining Multiple Information Sources to Solve Ill Posed Structure and Nanostructure Inverse Problems. *Acta Crystallogr. Sect. Found. Adv.* **2015**, *71* (6), 562–568. https://doi.org/10.1107/S2053273315014473.
(64) Beaucage, G. Approximations Leading to a Unified Exponential/Power-Law Approach to Small-Angle Scattering. *J. Appl. Crystallogr.* **1995**, *28* (6), 717–728. https://doi.org/10.1107/S0021889895005292.
(65) Doucet, M.; Cho, J. H.; Alina, G.; Attala, Z.; Bakker, J.; Bouwman, W.; Butler, P.; Campbell, K.; Cooper-Benun, T.; Durniak, C.; Forster, L.; Gonzalez, M.; Heenan, R.; Jackson, A.; King, S.; Kienzle, P.; Krzywon, J.; Murphy, R.; Nielsen, T.; O'Driscoll, L.; Potrzebowski, W.; Prescott, S.; Ferraz Leal, R.; Rozyczko, P.; Snow, T.; Washington, A. SasView Version 5.0.4, 2021. https://doi.org/10.5281/zenodo.4467703.